Supplemental Document

Biomedical Optics EXPRESS

Investigation of multiple scattering in space and spatial-frequency domains: with application to the analysis of aberration-diverse optical coherence tomography: supplement

MEIQI WU,[1] SIYANG LIU,[2] NICHALUK LEARTPRAPUN,[1] AND STEVEN ADIE[1,*]

[1]*Meinig School of Biomedical Engineering, Cornell University, Ithaca, NY 14853, USA*
[2]*School of Electrical and Computer Engineering, Cornell University, Ithaca, NY 14853, USA*
[*]*sga42@cornell.edu*

Supplement DOI: https://doi.org/10.6084/m9.figshare.16930285

Parent Article DOI: https://doi.org/10.1364/BOE.439395

Investigation of multiple scattering in space and spatial-frequency domains: with application to the analysis of aberration-diverse optical coherence tomography (supplementary material)

MEIQI WU,[1] SIYANG LIU,[2] NICHALUK LEARTPRAPUN,[1] AND STEVEN ADIE[1,*]

[1]*Meinig School of Biomedical Engineering, Cornell University, Ithaca, NY, 14853, USA*
[2]*School of Electrical and Computer Engineering, Cornell University, Ithaca, NY, 14853, USA*
**sga42@cornell.edu*

1. Multiple scattering randomization by AD-OCT

Aberration-diverse optical coherence tomography (AD-OCT) takes advantage of the difference in correlation properties between multiple scattering (MS) and single scattering (SS) signal under diversified illuminations. By introducing astigmatism of different angles to the illumination beams, AD-OCT generates different realizations of MS while maintaining the correction of SS signal after computational aberration correction. The diversity and randomization of AD-OCT is related to the introduced astigmatism magnitude. Larger aberration magnitude leads to larger randomization in the MS signal, and thus larger MS suppression with coherent averages.

In Visualization 1, we display the *en face* planes and cumulative coherent averages at four different depths comparing Gaussian control and AD-OCT with 160 μm line foci spacing. The four depths are 1 scattering length (l_s) in the scattering layer, 50 μm above the USAF target plane (6.4 l_s in the scattering layer), USAF target plane, and 5 coherence length (CL) below the USAF target plane (the MS depth). All of the images are after wobble correction and residual transverse shift correction, and are displayed with by their own color scale. For AD-OCT, the speckle pattern near the surface are mostly stable, but deep in the sample and at the MS depth, they are randomized with acquisition number or aberration state number *N*. The corresponding Gaussian *en face* planes at all depths would be stable across *N*. This is because AD-OCT randomizes the MS, and the level of MS in the scattering layer generally increases with depth.

For comparison, we also display the same information comparing Gaussian control and AD-OCT with 40 μm line foci spacing in Visualization 2. Similar to Visualization 1, for AD-OCT, the speckle pattern gets randomized deep in the sample and at the MS depth, but the level of randomization is less than the corresponding images in Visualization 1. The randomization in MS depends on the introduced astigmatism magnitude in the illumination beam. AD-OCT with 160 μm line foci spacing uses an illumination beam with larger astigmatism than AD-OCT with 40 μm line foci spacing, thus the MS gets more randomized than AD-OCT with 40 μm line foci spacing.

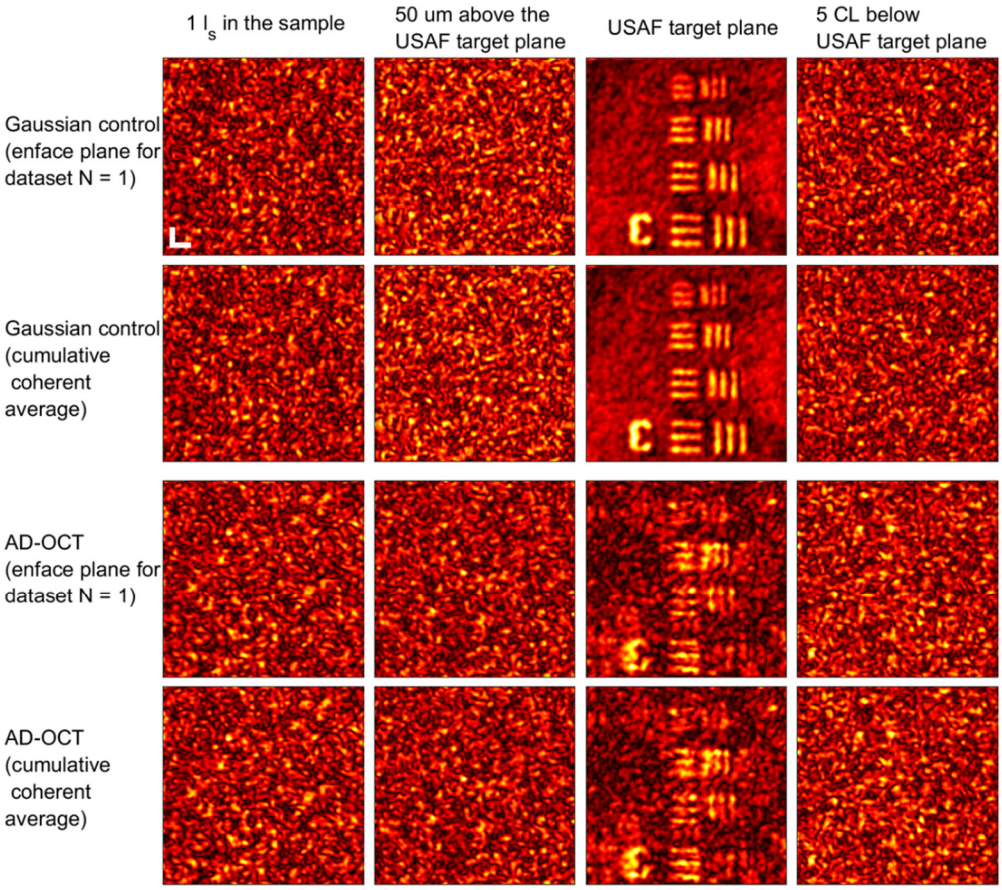

Visualization 1: En face planes and cumulative coherent averages at different depths comparing Gaussian control and AD-OCT with 160 μm line foci spacing. All the images are after wobble correction and transverse shift correction. Image of each panel in each frame is normalized by its own color scale. The scale bar represents 10 μm.

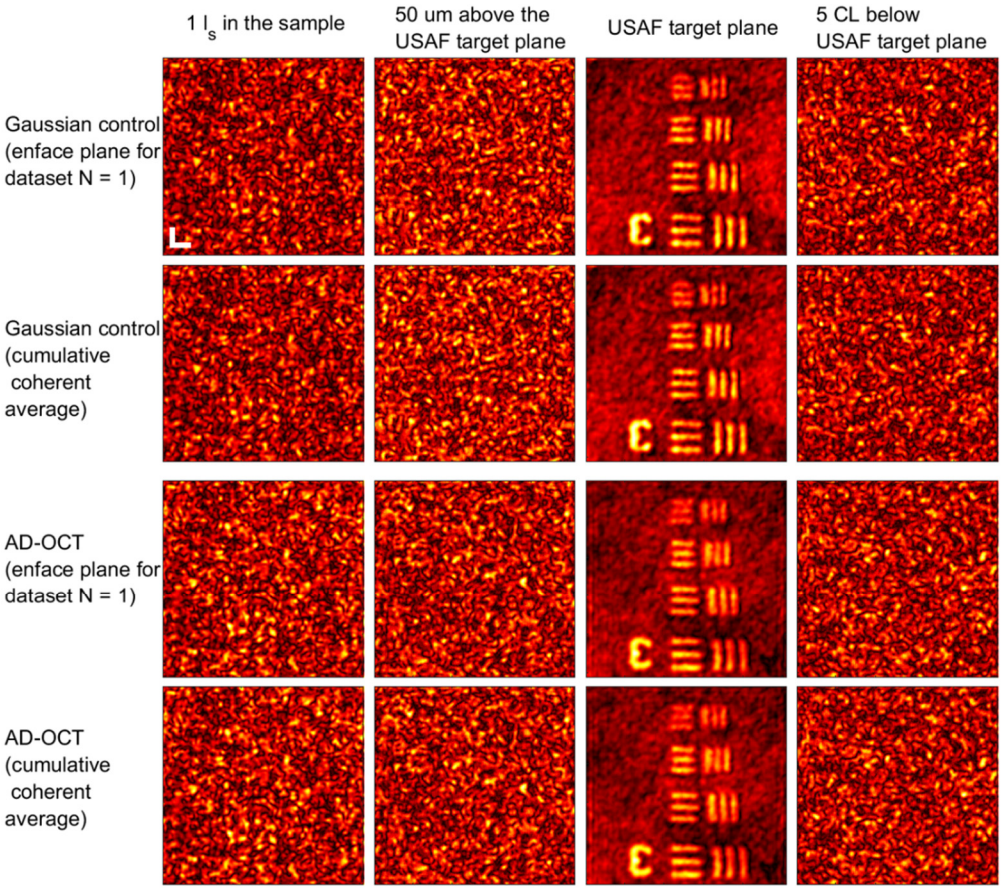

Visualization 2: *En face* planes and cumulative coherent averages at different depths comparing Gaussian control and AD-OCT with 40 μm line foci spacing. All the images are after wobble correction and transverse shift correction. Image of each panel in each frame is normalized by its own color scale. The scale bar represents 10 μm.

2. Transverse shift correction

Using the cross-correlation algorithm used in [1], we measured the depth-dependent residual transverse shifts in the scattering layer after wobble correction (Fig. S1(a-e)). However, due to the randomized speckle deep in the scattering layer, the algorithm fails at deep depths in the sample for AD-OCT with large foci spacing (i.e. 80 μm and 160 μm). Fortunately, from the measured depth-dependent transverse shifts in the resolution phantom, we found that the spatial shifts are very stable along depth (Fig. S1 (f)). Therefore, we detected spatial shifts in the scattering layer at the depths from 0 to 100 μm, took the average along depth, and used this information for transverse shift correction. Visualization 3 displays the *en face* planes before and after residual transverse shift correction across states at four different depths for AD-OCT with 160 μm line foci spacing. The four depths are 0.5 l_s in the scattering layer, 50 μm above the USAF target plane (6.4 l_s in the scattering layer), USAF target plane, and 5 CL below the USAF target plane (the MS depth).

The validation of the cross-correlation algorithm is shown in Fig. S1 (g). We applied known two-dimensional spatial shifts to an *en face* plane of an OCM dataset (0.5 l_s in the scattering layer, ~36 μm into the scattering layer), and calculated the relative shifts of the translated plane with respect to the original plane. From Fig. S1 (g), the detected shifts agree well with the applied shifts across 50 simulations.

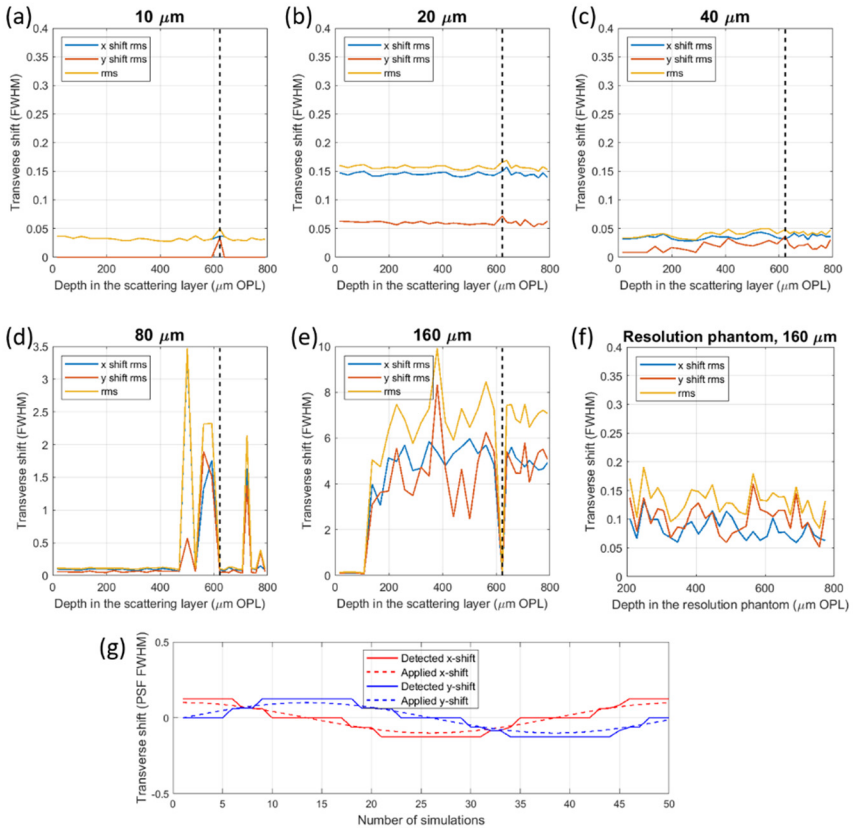

Fig. S1. (a-f) Root of mean squared (RMS) of measured depth-dependent transverse shifts along depth. The RMS at each depth is calculated across different astigmatic states. (a-e) are in the scattering layer for AD-OCT with different line foci spacing as labeled. The vertical dashed lines indicate the depth of USAF target plane in the scattering layer. (f) is in the resolution phantom for AD-OCT with 160 μm line foci spacing. (g) Validation of cross-correlation algorithm for spatial shifts detection.

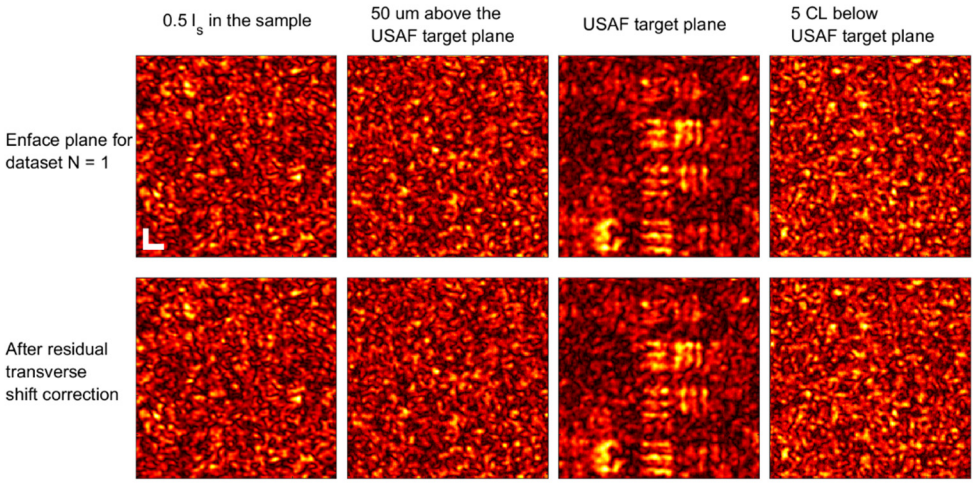

Visualization 3. *En face* planes before and after residual transverse shift corrections for AD-OCT with 160 µm line foci spacing. Image of each panel in each frame is normalized by its own color scale. The scale bar represents 10 µm.

3. Effect of residual transverse shifts on the depth-dependent spectral power of coherent averages

Although we corrected the residual transverse shifts after wobble correction, its effect on the coherent averages is still worth investigation. In order to quantify the effect of residual transverse shifts on the depth-dependent spectral signal after coherent averaging, we measured the transverse shifts across all the aberration states in the scattering layer for AD-OCT with 160 µm line foci spacing, applied the measured shifts to a single AD-OCT dataset with 160 µm line foci spacing, and calculated the depth-dependent spectral power of coherent averages (Fig. S2(a)). The power decay in the high-frequency region in Fig. S2 (a) is much smaller than the power decay we observed in the scattering sample with AD-OCT 160 µm line foci spacing (Fig. 14 (f)). We need to magnify the measured shifts by a factor of 4 to produce a similar level of decay to that observed in Fig. 14 (f) (see Fig. S2(b)). This indicates that the impact of the transverse shift correction on the depth-dependent signal after coherent averaging is not significant, suggesting that MS suppression rather than transverse shifts are the main cause of the depth-dependent signal drop in Fig. 14(f).

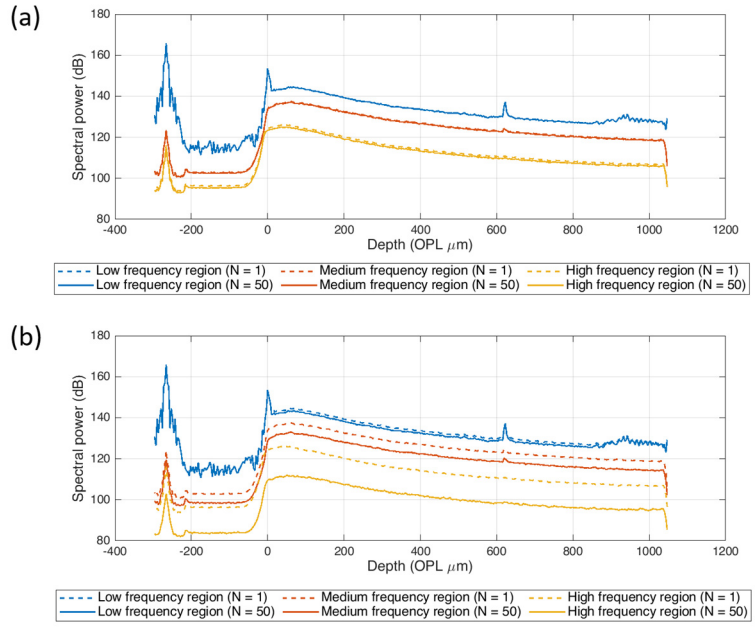

Fig. S2. (a) Depth-dependent spectral power of coherent averages of translated datasets. The original dataset is a single AD-OCT dataset with 160 µm line foci spacing, and the applied translations are the actual measured shifts across all the aberration states in the scattering sample with AD-OCT 160 µm line foci spacing. (b) Depth-dependent spectral power of coherent averages of translated datasets. The original dataset is a single AD-OCT dataset with 160 µm line foci spacing, and the applied translations are 4 times the actual measured shifts across all the aberration states in the scattering sample with AD-OCT 160 µm line foci spacing.

4. Standard deviation of SBR

The standard derivation of SBR is calculated by the error propagation formula using the standard deviation of signal and background.

$$\sigma_{\mathrm{SBR}} = \sqrt{\left(-\frac{S_{\mathrm{signal}}}{S_{\mathrm{background}}{}^{2}}\right)^{2}\sigma_{\mathrm{background}}{}^{2} + \left(\frac{1}{S_{\mathrm{background}}}\right)^{2}\sigma_{\mathrm{signal}}{}^{2}} \qquad \text{(Eq. S1)}$$

where σ_{SBR}, $\sigma_{\mathrm{background}}$ and σ_{signal} are the standard deviation of SBR, MS background and SS signal. S_{signal} and $S_{\mathrm{background}}$ are the signal and background as defined in Section 2.4. $\sigma_{\mathrm{background}}$ and σ_{signal} are calculated by the standard deviation of background and signal among 9 different groups of bars, respectively.

5. Effect of CAO on MS signal

In this work, we applied CAO at all the depths, including the cover glass and the USAF glass below the USAF target plane. As mentioned, we calculated the noise floor in the cover glass and the MS background in the USAF glass. The effect of CAO on the MS background and noise floor is worth investigation. Therefore, we plotted the noise floor and MS background with and without CAO in Fig. S3. We observed that CAO does not have much effect on the noise floor, but reduced the diversity of MS background. It seems that aberration correction makes some systematic contributions in the MS interference constructively.

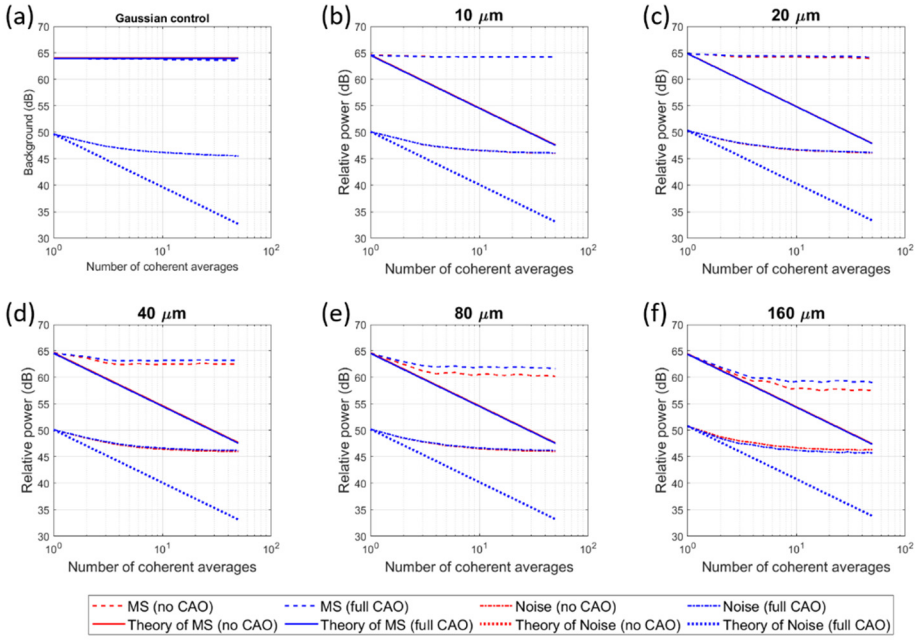

Fig. S3. The effect of CAO on the noise floor and MS signal. Noise floor and MS signal with and without CAO for (a) Gaussian control, (b) AD-OCT foci spacing = 10 μm, (c) AD-OCT foci spacing = 20 μm, (d) AD-OCT foci spacing = 40 μm, (e) AD-OCT foci spacing = 80 μm, (f) AD-OCT foci spacing = 160 μm.

6. Spatial-frequency domain analysis of a single standard OCM dataset

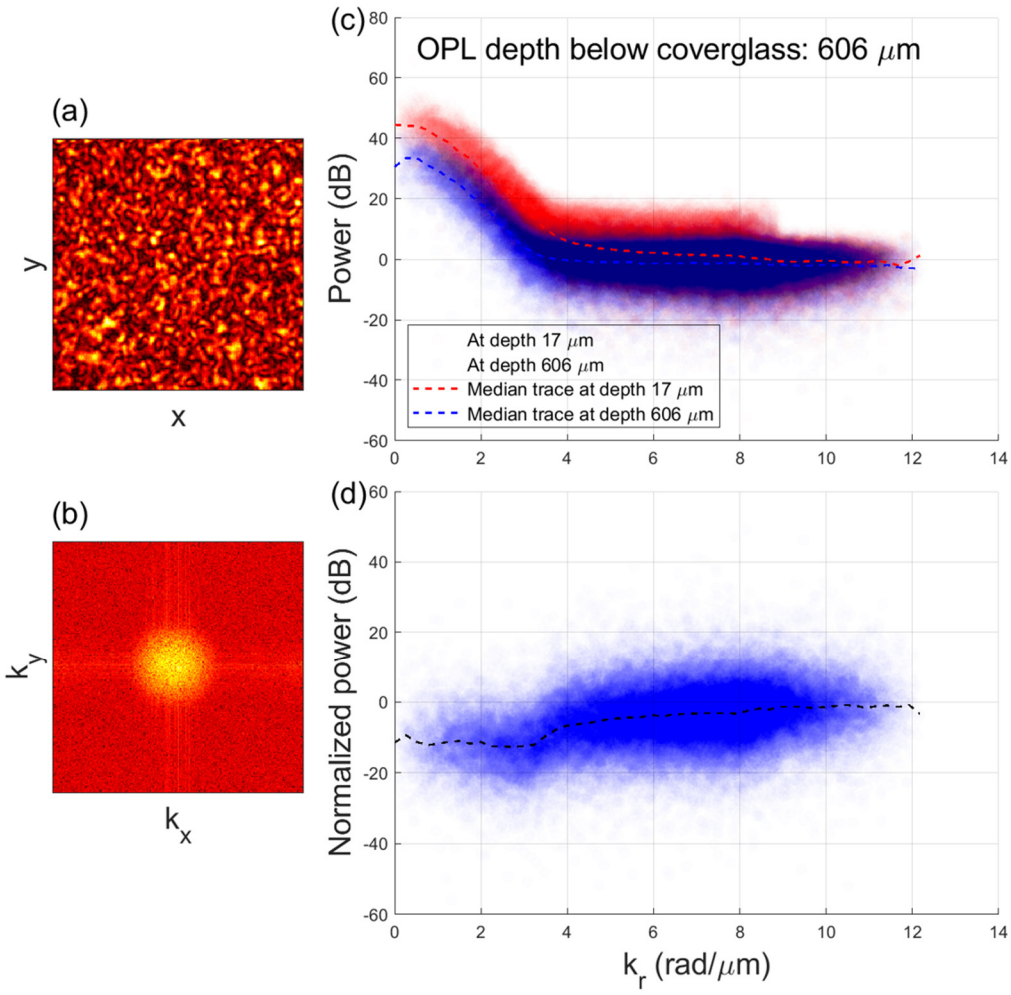

Visualization 4. Spatial-frequency domain analysis of a single standard OCM dataset. (a) *en face* plane of sample at the specified depth; (b) Fourier transform of (a); (c) spectral power at depth 17 μm and the specified depth in the scattering layer; (d) normalized spectrum power at the specified depth.

Funding

This research was supported in part by the National Science Foundation (CAREER: CBET-1752405), and the National Institutes of Health (NIBIB-R21EB022927, NINDS-R01NS120819).

Disclosure

The authors declare that there are no conflicts of interest related to the article.

References

1. M. Mujat, R. C. Chan, B. Cense, B. H. Park, C. Joo, T. Akkin, T. C. Chen, and J. F. De Boer, "Retinal nerve fiber layer thickness map determined from optical coherence tomography images," Optics Express **13**, 9480-9491 (2005).